Chapter 2
Representation of Texture

2.1 Introduction

As has been stated already, texture of a rolled sheet material is commonly represented as $\{hkl\}\ \langle uvw\rangle$, which means that most of the grains in the sheet material are such that their $\{hkl\}$ planes are nearly parallel to the rolling plane and the $\langle uvw\rangle$ directions of the grains are nearly parallel to the rolling direction. In practice, however, it may so happen that in a rolled sheet, a number of grains have their $\{h_1k_1l_1\}$ planes parallel to the rolling plane and their $\langle u_1v_1w_1\rangle$ directions parallel to the rolling direction; another few grains may have their $\{h_2k_2l_2\}$ planes parallel to the rolling plane and their $\langle u_2v_2w_2\rangle$ directions parallel to the rolling direction and so on. In that case, we say that the texture of the sheet material has a few components represented by $\{h_1k_1l_1\}\ \langle u_1v_1w_1\rangle$, $\{h_2k_2l_2\}\ \langle u_2v_2w_2\rangle$…, and so on. Such a complex texture can be represented as follows:

$$\text{Overall texture } = \sum w_i \cdot \{hkl\}_i \cdot \langle uvw\rangle_i \tag{2.1}$$

Here, w_i is a weighting factor that is introduced to allow for the relative intensities or strengths of the different components. Broadly speaking, there are two ways of representing texture: the pole figure method and the orientation distribution function (ODF) method.

2.2 Pole Figure Method

A pole figure is a two-dimensional stereographic projection in which the positions and intensities of specific crystallographic orientations are plotted in relation to the specimen geometry.

We shall first discuss the salient features of a stereographic projection, which is essential to understand a pole figure. A stereographic projection is a two-dimensional

S. Suwas and R. K. Ray, *Crystallographic Texture of Materials*,
Engineering Materials and Processes, DOI: 10.1007/978-1-4471-6314-5_2,

projection of a three-dimensional crystal (or unit cell) such that the angular relationships between different planes, different directions and between planes, and directions in the crystal (or unit cell) can be easily read out from the projection. Thus, a stereographic projection is an "angle-true" projection in just the same way as a geographic atlas is a two-dimensional "area-true" projection of the three-dimensional globe. The procedure for drawing a stereographic projection for a cubic crystal (or unit cell) is outlined below.

2.2.1 Stereographic Projection

Let us consider a very small unit cell, so small that it can be taken as a point. Construct a big sphere, called the reference sphere, around the point unit cell taken as the center. Next, we draw perpendiculars to the six cube faces of the unit cell and extend these till they cut the reference sphere. These points of intersection of the plane normals with the reference sphere are known as the poles of the respective cube planes, (100), $(\bar{1}00)$, (010), $(0\bar{1}0)$, (001) and $(00\bar{1})$. These poles have all been marked in Fig. 2.1a.

We then place a source of light, say at the 001 pole position and then allow the light rays passing through the poles 100, $\bar{1}00$, 010 and $0\bar{1}0$ to fall on a piece of paper put perpendicular to the 001-$00\bar{1}$ axis. The lower half of the reference sphere will then be projected as a circle, known as the basic circle on the piece of paper which is nothing but the projection plane, parallel to the (001) plane of the unit cell. The pole 001 will be at the center of the basic circle, while the poles 100, $\bar{1}00$, 010 and $0\bar{1}0$ will appear on the periphery of the basic circle, as shown in Fig. 2.1b. The basic circle, along with the poles of the different {100}-type planes is nothing but a stereographic projection of the three-dimensional unit cell, placed at the center of the reference sphere. Since the plane of the projection is parallel to the (001) plane, the projection is known as the (001) stereographic projection of the cubic unit cell. We can easily verify whether this projection is really an "angle-true" projection or not. For example, in the projection, the angle between the poles 100 and 010 is 90°; again, the angle between the planes (100) and (010) in the cubic unit cell is also 90°. In this way, it can be verified by considering two planes or two directions or a plane and a direction that the stereographic projection is really an "angle-true" projection.

In the projection given in Fig. 2.1b, the poles of only the {100}-type planes of the cubic unit cell have been plotted. Sometimes, we need to have stereographic projections showing the poles of more than one type of plane. In general, such projections, which contain the projected poles of many crystallographic planes, are known as "standard projections." Figure 2.2a shows such a standard stereographic projection for a cubic unit cell showing the poles of {100}, {110}, and {111} planes, with (001) as the plane of projection. In a similar manner, the poles of the {100}, {110}, and {111} planes can also be plotted with, say (110) and (111), as the projection planes, and the resulting stereographic projections (or stereograms)

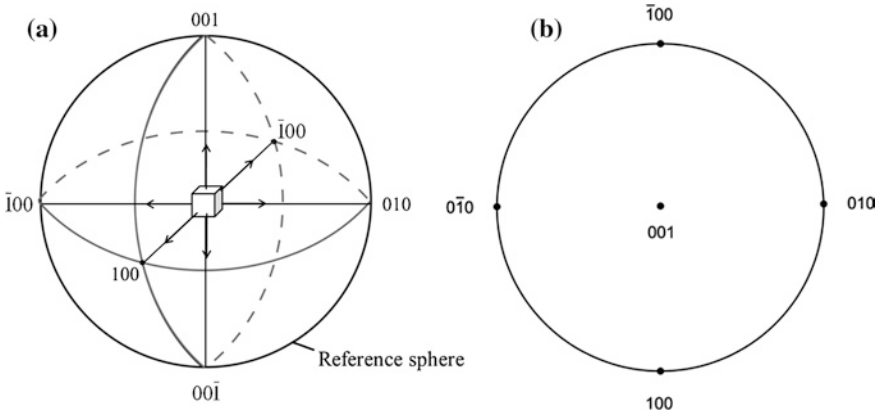

Fig. 2.1 Schematic representation of stereographic projection. (**a**) Plane normals of the cube present at the center of the reference sphere intersect with the surface of the sphere and provide the poles (100), ($\bar{1}$00), (010), (0$\bar{1}$0), (001), and (00$\bar{1}$). (**b**) The basic circle from (**a**) depicting the (001) stereographic projection

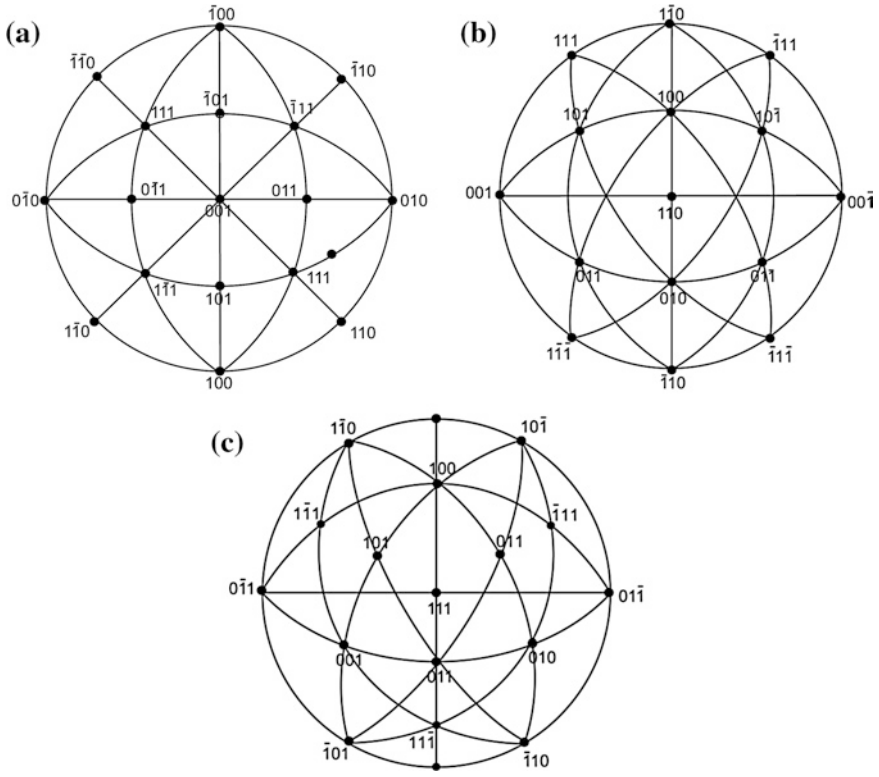

Fig. 2.2 **a** (001), **b** (110), and **c** (111) stereograms for cubic materials

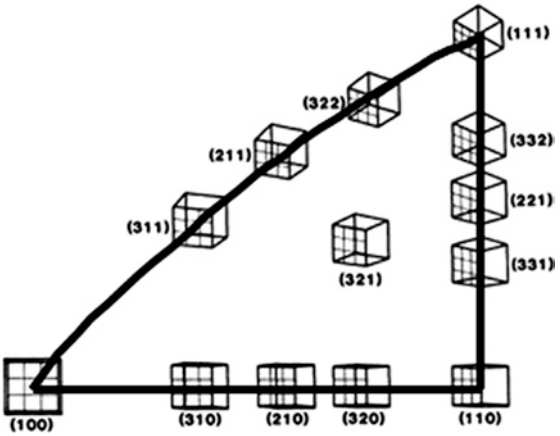

Fig. 2.3 Standard unit stereographic triangle for cubic crystal system superimposed with crystal orientations. After [1]

are shown in Fig. 2.2b and c. As will be described later in this chapter, standard stereographic projections can be very useful to identify texture in a pole figure.

Due to the symmetry of the cubic crystal structure, the stereographic projection can be divided into 24 equivalent triangles. The three corners of each triangle are the projected poles of {100}, {110}, and {111} (see Fig. 2.2). Figure 2.3 depicts one such triangle in the (001) projection. Each point on this projection represents a unit-cell orientation.

Such projections can also be drawn for the poles of as many planes as required and with any (*hkl*) plane as the plane of projection. In fact, nowadays, standard softwares are available for drawing stereographic projections for any type of crystal on any (*hkl*) plane.

2.2.2 Pole Figure

We shall illustrate here the principle involved in drawing a pole figure, by considering a rolled sheet of a cubic material. A rectangular piece of such a sheet material is associated with three mutually perpendicular specimen parameters, namely the normal direction (ND), which is perpendicular to the sheet plane, the rolling direction (RD), and the transverse direction (TD). If we imagine that the specimen is very small, almost like a point, and place it at the center of a big reference sphere (Fig. 2.4a), then following the procedure adopted for drawing a stereographic projection, we can have a projection (parallel to the sheet surface), where ND will be at the center and RD and TD will be on the periphery of the projection, as shown in Fig. 2.4b. Again, let us consider the three mutually perpendicular planes (100), (010), and (001) of a rectangular specimen, as shown in Fig. 2.4c. Let the normals to these three planes be extended to intersect the reference sphere at the three x-marked points (Fig. 2.4c). Obviously, these three plane normals will be mutually perpendicular to one another.

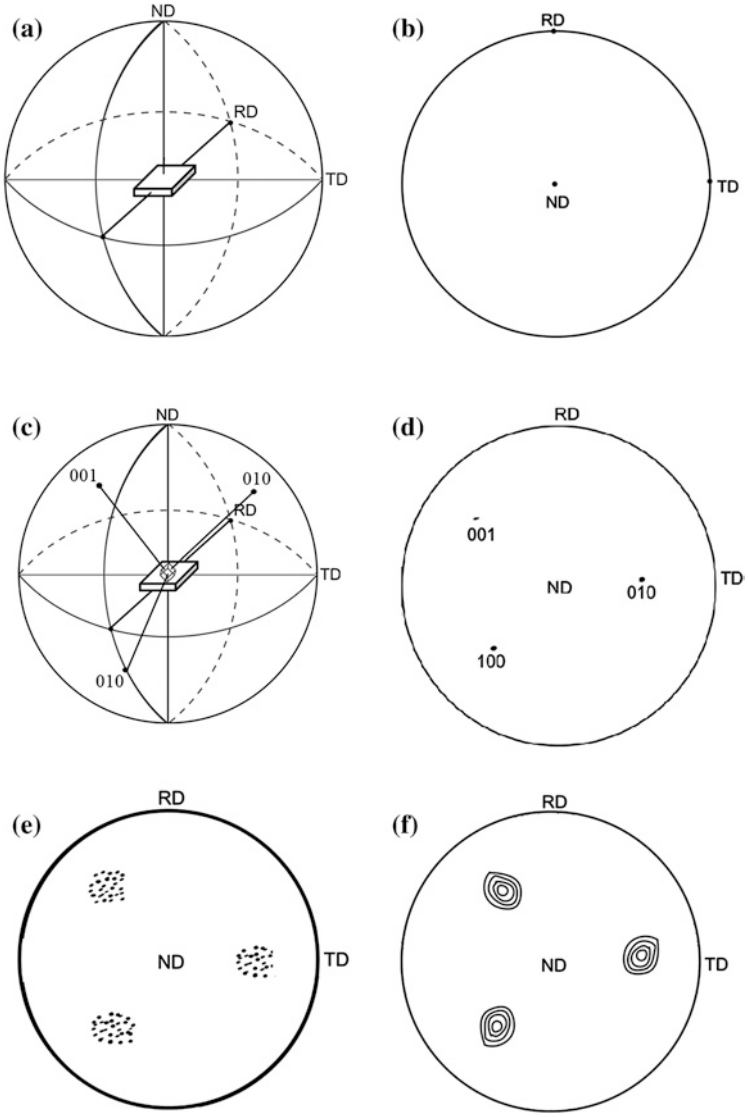

Fig. 2.4 **a** Projection plane and reference sphere with a rolled sheet at the center. **b** Projection of the poles RD, TD, and ND on the reference plane constituting the sample reference frame of a pole figure. **c** The points of intersection of the normal to the plane (100), (010), and (001) of the specimen on the reference sphere. **d** The three poles 100, 010, and 001, as projected on the basic circle. **e** Clustering of projected poles of (100), (010), and (001) planes from the different grains of the specimen. **f** Pole densities shown as *contour lines*

The points 100, 010, and 001 in Fig. 2.4c are nothing but the poles of the planes with these three sets of indices. Again, we project these poles on a projection plane which

is parallel to the surface of the specimen, as shown in Fig. 2.4d. Clearly, this diagram is a stereographic projection showing both the specimen parameters ND-RD-TD and the crystallographic parameters 100-010-001.

Now, let us take into account all the 100, 010, and 001 poles from the different grains in the sheet specimen and draw the projections of those poles on the given projection plane. If it so happens that most of the projected poles are clustered together, as shown in Fig. 2.4e, it will indicate that the material is textured. If, on the other hand, the projected poles are distributed rather uniformly, then it will indicate that the material is textureless or random. Figure 2.4e is nothing but a pole figure of the given sheet material. Normally, the pole densities in a pole figure are represented not as discrete points, as shown in Fig. 2.4e, but by way of some contour lines, as shown in Fig. 2.4f. The number against each contour line represents the density of poles relative to that which would be expected for a specimen which is textureless or random. Whereas, contour lines greater than 1 times random will signify a concentration of poles; contour lines less than 1 times random will imply a depletion of poles. Figure 2.4f is a {100} pole figure of a cubic material which shows the spatial locations of only the {100}-type planes in the material with respect to the locations of the specimen parameters. In a similar way, the {111}, {110}, etc. pole figures for the same material can also be determined.

In real-life situation, the number of grains in a specimen, generally, will be rather large and, therefore, the determination of individual orientations will be impractical. The normal practice these days is to collect orientation data from many grains simultaneously (using X-ray or neutron diffraction) or collect the individual grain orientation data (using electron diffraction) and combine them to present in the form of density contours on the pole figure. The exact experimental methods for drawing a pole figure will be described in detail in Chap. 3.

2.2.3 Interpretation of a Pole Figure

Figure 2.5a shows the pole densities of the {111} type of planes in a heavily rolled and recrystallized sheet sample of Ni, plotted in the form of a pole figure, which also shows the locations of the specimen parameters: RD, TD, and ND. The pole figure clearly indicates that the material is highly textured, with high densities of {111} poles lying clustered at distinct locations of the pole figure. Now, the question is how to read the texture plot in terms of identifying the texture components, as represented in this pole figure.

As mentioned earlier, standard stereographic projections can be very useful to identify the texture from a pole figure. For example, in this particular case, if we superimpose the standard (001) stereographic projection of a cubic material (Fig. 2.5b) on this pole figure (Fig. 2.5c), we observe that the locations of the highest pole densities in the pole figure lie at the specific {111} positions of the standard stereographic projection. Now, in the above pole figure, only the {111} poles have been plotted. If it so happens that most of the grains in the specimen of

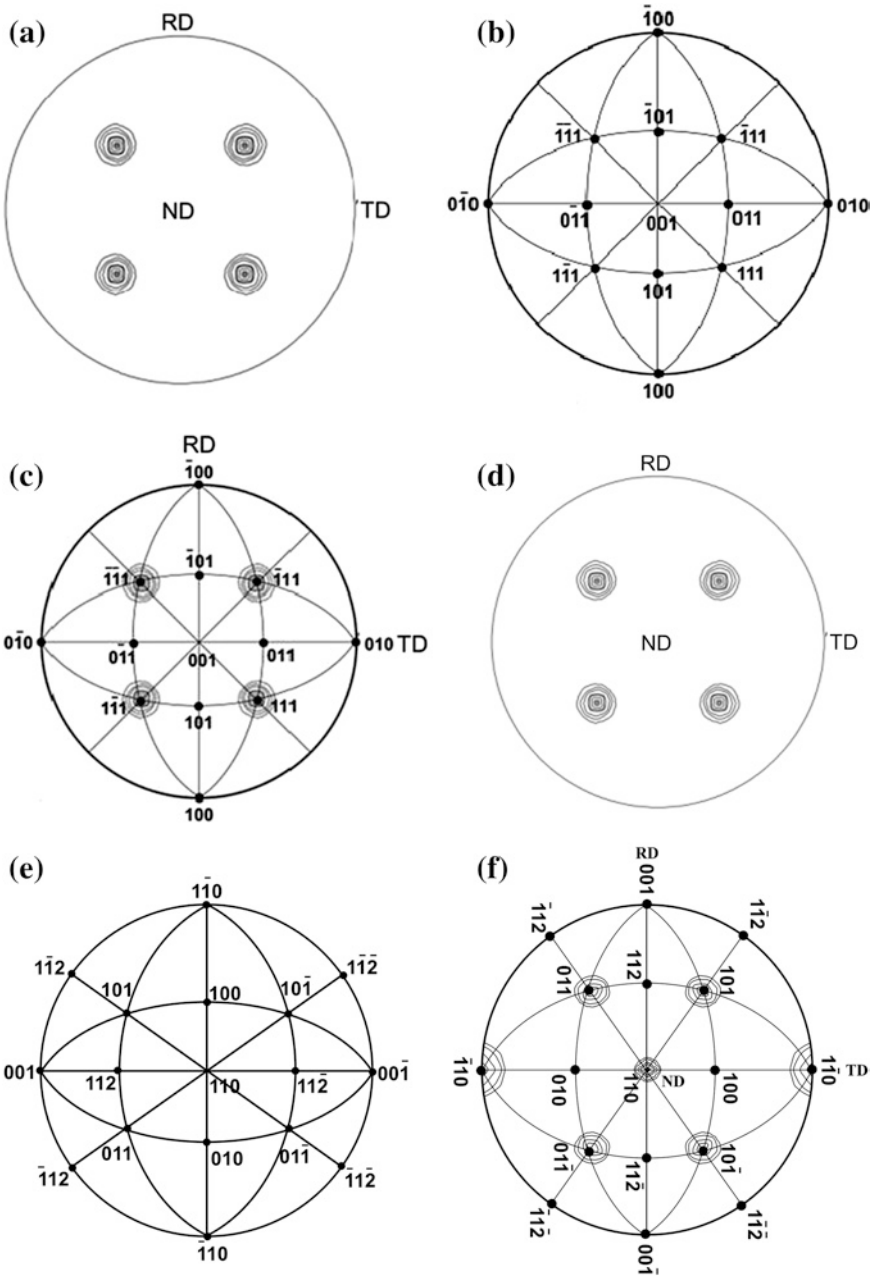

Fig. 2.5 **a** {111} pole figure for a rolled sheet. **b** (001) stereographic projection, and **c** pole figure and stereographic projection in **a** and **b** are superimposed with each other, which shows that (001) is the rolling plane and $[0\bar{1}0]$ is the rolling direction. **d** {110} pole figure for a rolled sheet. **e** (110) standard stereographic projection, and **f** pole figure and stereographic projection in **d** and **e** are superimposed on each other

Ni are such that their {111} planes lie parallel to the sheet plane, in that case, all the plane normals would be pointing toward ND and, therefore, the highest pole densities would have been obtained in and around ND, i.e., at the central region of the pole figure. The very fact that the highest pole densities lie shifted from the central region indicates that it is not {111}, but some other {hkl} planes of most of the grains which must be lying parallel to the sheet plane (the rolling plane).

When we superimpose the standard (001) stereographic projection on {111} pole figure of Ni, it implies that the projection plane for the stereogram [which is (001)] is the same as the projection plane of the pole figure, which is nothing but the sheet plane. And under this condition, the high-pole density locations in the pole figure correspond unambiguously to the {111} locations of the standard (001) stereographic projection. It means that we can account for the high-pole density regions of the pole figure only if the sheet plane is (001). Under these conditions, the RD of the pole figure lies exactly at the $[\bar{1}00]$ location of the standard stereogram. Hence, the texture of Ni, as represented in the pole figure, can be described as (001) $[\bar{1}00]$. This is a very simple case of indexing a pole figure. There could be situations where the {111} pole densities in the given pole figure may not coincide with the {111} locations in the standard stereogram. Or, let us say, the {110} pole densities in a given pole figure may not, at the first instance, coincide with the {110} locations of a standard stereogram. In that case, pole figure needs to be rotated around ND relatively to the relevant stereogram to make the poles coincide. Such a situation is depicted in Fig. 2.5d–f. In this particular case, the texture can be easily read as (110) [001]. This example clearly conveys that any suitable standard stereogram can be used to index the texture components.

It is to be mentioned here that identification of the texture components for hexagonal materials by the above method has some limitations. The pole figures basically describe the crystallographic directions (plane normals). In the hexagonal system, the Miller-Bravais indices for many planes are not the same as their normals; hence, the indexing of texture components $\{hkil\}\ \langle uvtw\rangle$ becomes complicated. In such cases, a double stereogram needs to be used (Fig. 2.6) which contains the projections of both plane normals and rational directions.

2.2.4 Pole Figures Showing Ideal Orientations

For the interpretation of pole figures, it is necessary to have the locations of some important ideal orientations in pole figure form. Figure 2.7a presents a series of (200) pole figures, showing the ideal positions of a few important texture components that are encountered in FCC and BCC materials [3]. The B {110} ⟨112⟩, C {112} ⟨111⟩, and S {123} ⟨634⟩ components, shown in Fig. 2.7a, are normally found in the deformation texture of FCC materials. Recrystallized FCC materials show a predominantly cube {100} ⟨001⟩ component. The components {332} ⟨113⟩ and {113} ⟨110⟩, shown in Fig. 2.7b, are the major transformation texture components of BCC steel (ferrite), which are obtained from the

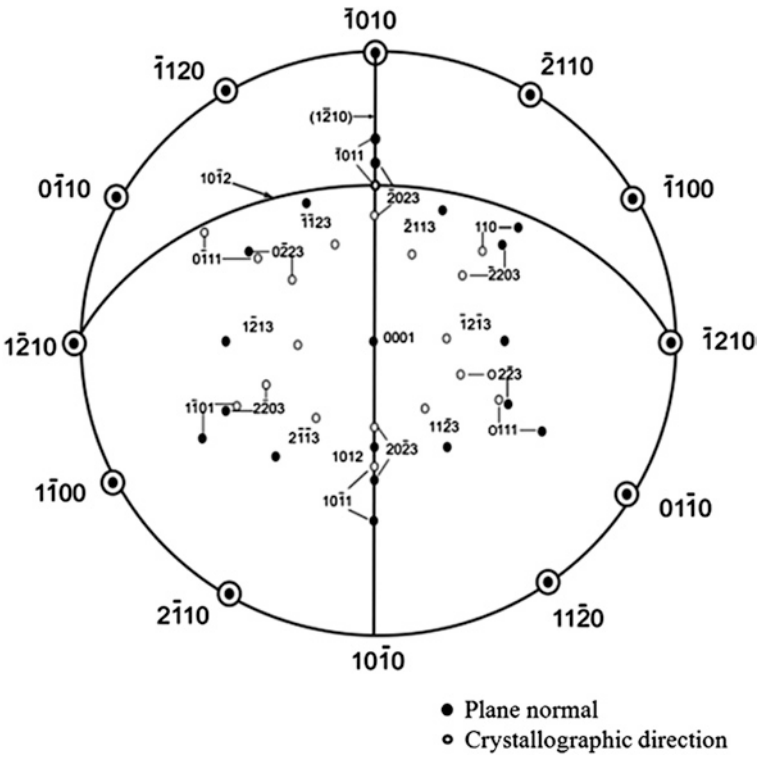

Fig. 2.6 (0001) double stereogram of titanium. After [2]

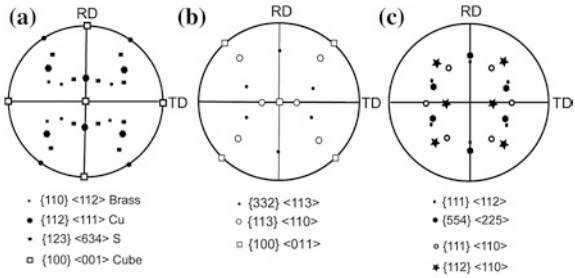

Fig. 2.7 Standard (200) pole figures showing ideal texture components (**a**) deformation and recrystallization components of a FCC material and (**b** and **c**) major texture components in a transformed BCC material from FCC material plus some important components of the rolling and recrystallization texture of ferrite. After [3]

deformation texture components of parent austenite phase. Similarly, the component $\{100\}\ \langle 011\rangle$ is obtained from the cube $\{100\}\ \langle 001\rangle$ component of recrystallized austenite upon transformation to ferrite. Again, the components $\{111\}\ \langle 112\rangle$,

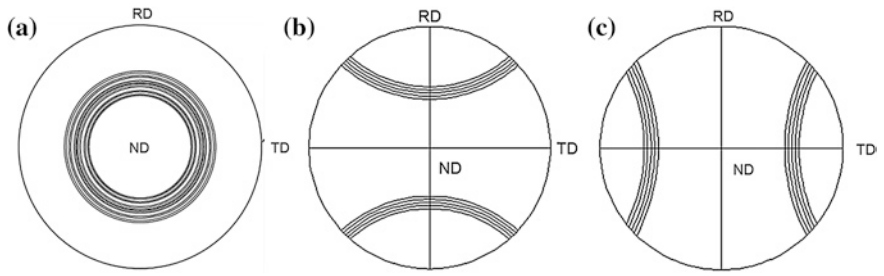

Fig. 2.8 (001) Pole figure showing (110) fiber along. **a** ND, **b** RD, and **c** TD

{554} ⟨225⟩, {111} ⟨110⟩, and {112} ⟨110⟩ presented in Fig. 2.7c are some of the important texture components in cold-rolled and recrystallized BCC low-carbon steels (ferrite).

We can as well plot important ideal orientations in terms of {111}-, {110}-type pole figures, etc. It is quite apparent that plots of such ideal texture components will be very much useful in identifying the texture component(s) present in experimental pole figures.

2.2.5 Pole Figures Showing Fiber Texture

So far, in a pole figure, we have shown textures in terms of one or more components, centered around ideal orientations. Such components are also known as peak-type components. Very often, as in the wire-drawing operation, textures are produced by axially symmetric deformation. Such textures usually exhibit rotational symmetry, and as such, these can be described by specifying the crystallographic direction ⟨*uvw*⟩, which is parallel or nearly parallel to the axis of deformation. Such textures are called fiber textures, and the axis is called the fiber axis. The components belonging to a fiber texture can be obtained by rotation about the fiber axis, and such type of texture can be represented in the pole figure by continuous bands of orientations, as shown in Fig. 2.8.

In Fig. 2.8, ⟨110⟩ fiber textures have been shown by bands of orientations in a (001) pole figure. If the bands are populated uniformly by orientations, then it is a perfect fiber. When these are populated only partially, the result is a partial fiber texture.

Sometimes, fiber textures are observed in materials that may not have been deformed by processes that are axially symmetric. In fact, such a situation sometimes occurs in rolled as well as rolled and annealed sheet materials, where the texture may often be best described in terms of not one but several fibers.

It must be stated here that the textures formed in actual materials may be far more complex to be described in terms of perfect peak-type components or perfect fibers or both. In fact, multicomponent textures are very common in practice.

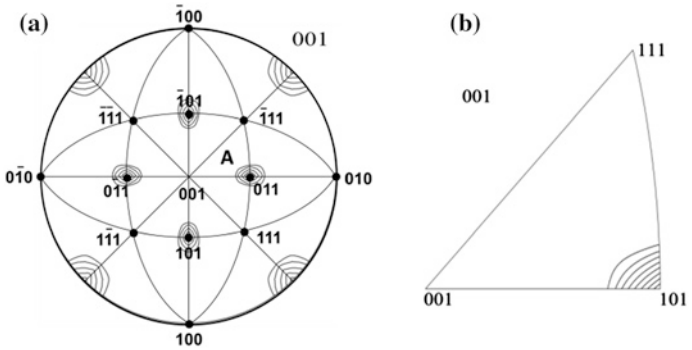

Fig. 2.9 **a** A complete 001 inverse pole figure, showing ⟨110⟩ parallel to the wire axis, superimposed on a standard (001) stereogram. **b** A unit stereographic triangle A has been separated out

2.2.6 Inverse Pole Figures

The most common method of representing textural data for materials is by drawing the conventional pole figures. However, sometimes, satisfactory description of texture can also be given in terms of an inverse pole figure, in which the distribution of a selected direction in the specimen, in relation to the crystal axes, is depicted. As it appears from the name itself, the representation in an inverse pole figure is exactly inverse of the pole figure. Here, sample directions are projected into the crystal frame as opposed to pole figures which are essentially the projection of crystallographic directions in the sample frame of reference. The inverse pole figures are sometimes also called the axis distribution charts. The projection plane for an inverse pole figure is a standard projection of the crystal, of which only the unit stereographic triangle needs be shown. For cubic crystal symmetry, in the stereographic projection, 24 unit triangles are crystallographically similar (Fig. 2.9a). Therefore, the data represented over 1/24th of the complete stereographic projection are sufficient for inverse pole figure representation (Fig. 2.9b).

Figure 2.9b shows the 001 inverse pole figure for the wire axis. Here, the contour lines effectively show the frequency with which the given specimen direction, here the wire axis, more or less coincides with the crystallographic axes, ⟨100⟩, ⟨110⟩, and ⟨111⟩. The figure shows that most of the grains in the wire have their ⟨101⟩ axis nearly aligned toward the wire axis.

When a material is subjected to axisymmetric deformation, where deformation processes are such that only one axis needs to be specified, such as in case of a wire or an extruded rod, an inverse pole figure can depict the texture quite satisfactorily.

Inverse pole figures can be used to represent rolled sheet textures also. However, here, three separate projections are required to show the distribution of three specimen axes, namely the normal direction (ND), the rolling direction (RD), and the transverse direction (TD). The three inverse pole figures for a 95 % cold-rolled nickel are shown in Fig. 2.10.

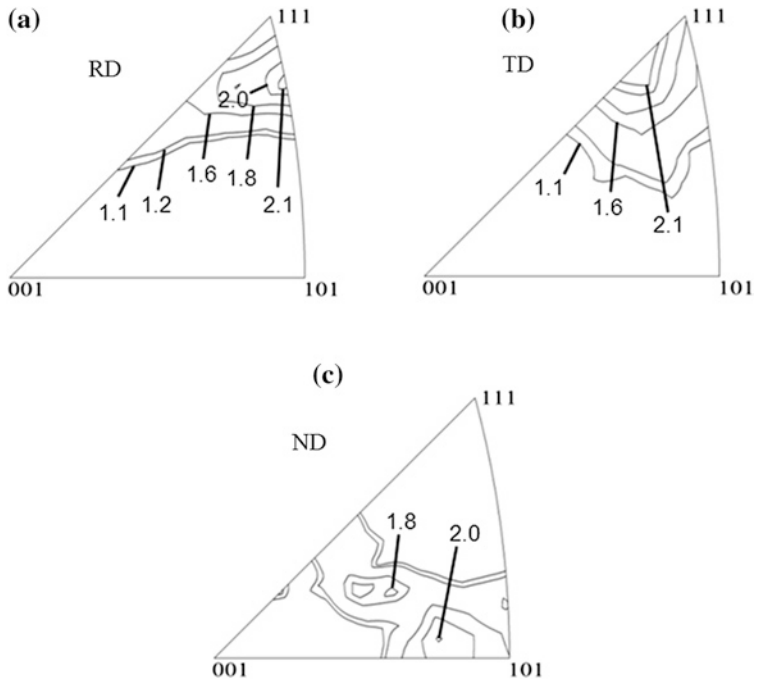

Fig. 2.10 Inverse pole figures of 95 % cold-rolled nickel for **a** RD, **b** TD, and **c** ND (*Courtesy* R. Madhavan)

2.3 Orientation Distribution Function (ODF) Method

As stated earlier, a pole figure is a two-dimensional stereographic projection, in which poles of a particular crystallographic plane (*hkl*) from an aggregate of grains or crystals in a polycrystalline material are specified relative to the specimen geometry. Although pole figures provide a useful description of the texture present in a material, the information that could be extracted from pole figure is insufficient and at best semi-quantitative. This is due to the fact that the crystal is a three-dimensional entity and pole figure representation has only two angles (α, β) to describe the crystal orientation (Fig 2.11). This leads to poor resolution of the orientation distribution on a pole figure. This problem can be mitigated by the use of the orientation distribution function (ODF).

The ODF method is based on describing a crystal orientation in a way which is completely different from the traditional description of an orientation in the form $\{hkl\}\ \langle uvw\rangle$. The orientation distribution function is a mathematical function that describes the frequency of occurrence of particular crystal orientations in a three-dimensional Euler space whose coordinates are defined by three Euler angles. These angles result from three consecutive rotations that are needed to be given to each crystallite in the specimen, in order to bring its crystallographic axes into coincidence with the specimen axes. The details regarding these rotations will be described in the next section. The complete description of orientation will then consist of the

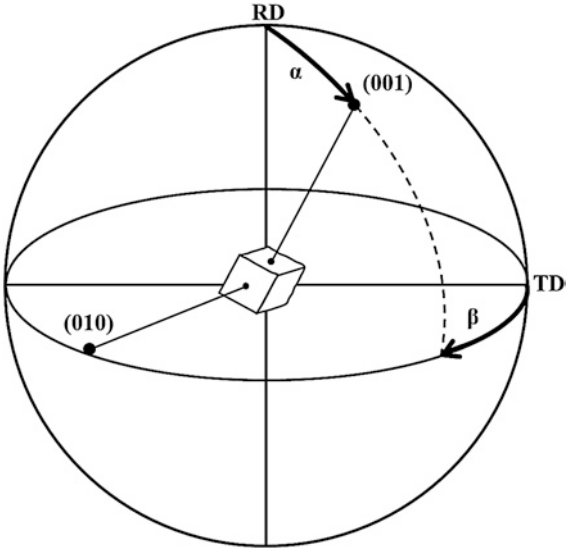

Fig. 2.11 Schematic showing the two degrees of freedom (α, β) for an orientation in a pole figure

sets of rotations related to all the crystallites in the specimen. Several mathematical formulations have been developed which allow a mathematical function to be calculated from the numerical data obtained from pole figures that could describe the orientation of all the crystallites in a polycrystalline material collectively in a more appropriate manner. Such procedures have been proposed independently by Bunge [4], Roe [5], and Williams [6, 7]. While Williams used an iterative least squares solution, both Roe and Bunge used generalized spherical harmonic functions to calculate the ODF. All these methods involve defining an orientation by three independent parameters (Euler angles) in just the same way as the traditional description of an orientation in the form $\{hkl\}\ \langle uvw \rangle$. There are two main methods for reconstructing an orientation distribution function based on pole figure data: (i) harmonic method that fits the coefficients of spherical harmonic functions to the data, and (ii) discrete method that calculates orientation distribution directly in discrete representation via an iterative process. It is a two-step method. The first step involves fitting coefficients to the available pole figure data. The intensity p at any angular position (α, β) on a pole figure is given by the following expression:

$$p(\alpha, \beta) = \Sigma_{l=0}^{\infty} \Sigma_{m=-l}^{l} Q_{lm} P_l^m \cos\alpha e^{im\beta} \tag{2.2}$$

where, Q_{lm} are the coefficients to be determined, α, β are the declination and azimuthal angle, P are the associated Legendre polynomials and l and m are the integers that determine the shape of the function. Since the functions in the above equation are orthogonal, it can be re-written as:

$$Q_{lm} = \int_0^m \int_0^{2\pi} p(\alpha, \beta) P_l^m(\cos\alpha) e^{-im\beta} \sin\alpha d\beta d\alpha \tag{2.3}$$

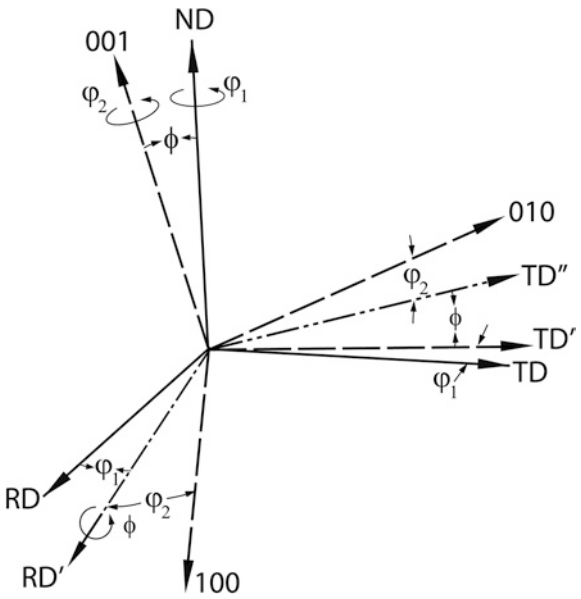

Fig. 2.12 Schematic representation of Euler angles, as defined by Bunge. After [8]

2.3.1 *Description of an Orientation by the Euler Angles φ_1, Φ, and φ_2*

All the three methods proposed by Bunge, Roe, and Williams employ different definitions and use different symbols to describe the orientation of a given crystallite. Out of the three, the Bunge notation is the one which is most commonly used. Here, for a flat-rolled sheet material, the specimen geometry can be defined by three mutually perpendicular directions, ND, RD, and TD, the so-called specimen frame (S). Similarly, for a grain or crystallite in a cubic material, a crystallographic frame (C) can be defined by the set of three mutually perpendicular axes, [100], [010], and [001]. The determination of orientation of the given grain will then involve the three rotations that are necessary to transform the specimen frame (S) into the crystallographic frame (C) of the grain. The series of three rotations, suggested by Bunge, are as follows (See Fig. 2.12).

1. A first rotation by an angle φ_1 is to be given around ND, which will take RD to the position RD′ and TD to TD′. The amount of the angle φ_1 should be such that RD′ will be perpendicular to the plane formed by ND and [001].
2. A second rotation by an angle Φ is to be given around RD′; the amount of Φ should be such that ND becomes coincident with [001]. By this process, TD′ will assume the position TD″.
3. A third rotation by an angle φ_2 is to be given around (ND = [001]), the amount of φ_2 being such that by this rotation RD′ goes to [100] and TD″ into [010].

According to the scheme proposed by Bunge, a set of (φ_1, Φ, φ_2) values signifies the orientation of a crystal.

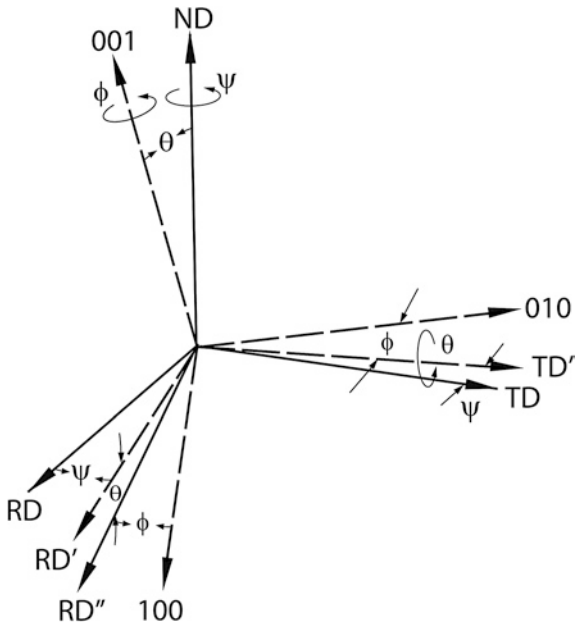

Fig. 2.13 Three consecutive Euler rotations defining an orientation based on Roe convention. After [5]

The three Euler angles, suggested by Roe to define an orientation, are shown in Fig. 2.13. Here, the two angles θ and ϕ together fix the position of the sheet normal direction (ND) with respect to the crystal axes, 001–010–100 as shown. Obviously, the rolling direction (RD) of the sheet will then lie on a great circle at 90° to ND and can be defined by a third Euler angle ψ. Therefore, according to Roe's notation, the three Euler angles which describe an orientation are φ, θ, and ψ.

According to Williams's notation, the relevant Euler angles are α, ρ, and β. The relationship between these three sets of notations is as follows:

Bunge	Roe	Williams
$\varphi_2 + \pi/2$	ϕ	α
Φ	θ	ρ
$\varphi_1 - \pi/2$	ψ	$\beta = \psi + \tan^{-1}(\tan\alpha \cos\rho)$

The set of three angles, as derived above, can describe a three-dimensional orientation space, in which each point represents a particular crystal, whose orientation is represented by the value of the three Euler angles at that point. The original treatment of ODF analysis was developed for materials with cubic crystal structure and orthorhombic specimen symmetry, which is applicable to sheet products. However, at a later stage, the same treatment has been successfully applied to materials with lower crystal symmetry, e.g., hexagonal and orthorhombic crystal symmetries and also for the processes that involve sample symmetries other than orthorhombic.

2.3.2 The Orientation Distribution Function

Polycrystalline materials consist of crystallites of different shape, size, and orientation. In the present context, orientations are the main distinguishing features for the crystallites. Each crystallite can be represented by a specific set of Euler angles, defined above, and the orientation of the crystallite 'g' can be written as

$$g = g(\varphi_1, \Phi, \varphi_2) \tag{2.4}$$

If we assume that all the crystallites, having an orientation "g" and with the spread of "Δg," are contained within a volume "ΔV" and if "V" is the total volume of the sample, then an orientation distribution function $f(g)$ can be defined as follows

$$f(g)\mathrm{d}g = \frac{\Delta V}{V} \tag{2.5}$$

The orientation parameters, φ_1, Φ, and φ_2, can be used as three Cartesian coordinates to define a three-dimensional orientation space. Each point within this space will have a specific value (φ_1, Φ, and φ_2) and as such will represent an orientation of a crystal or grain with respect to the specimen frame of reference. Cluster of such points within the orientation space will indicate presence of a texture in the material. If, on the other hand, such points are scattered in a random fashion, it will signify that the material is textureless.

According to Bunge and Morris [9], the density of the points distributed within the three-dimensional orientation space can be represented by an orientation distribution function (ODF), which may be expressed as a series of generalized spherical harmonics of the form:

$$f(\varphi_1 \Phi \varphi_2) = \sum_{l=0}^{\infty} \sum_{m=-l}^{+l} \sum_{n=-l}^{+l} \boldsymbol{C_l^{mn} T_l^{mn}(g)} \tag{2.6}$$

$$\text{or,} \quad f(\varphi_1 \Phi \varphi_2) = \sum_{l=0}^{\infty} \sum_{m=-l}^{+l} \sum_{n=-l}^{+l} \boldsymbol{C_l^{mn} P_l^{mn}(\Phi) e^{-im\varphi_2} e^{-in\varphi_1}} \tag{2.7}$$

where $\boldsymbol{C_l^{mn}}$ are the. series coefficients and $\boldsymbol{P_l^{mn}(\Phi) e^{-im\varphi_2} e^{-in\varphi_1}}$ are certain generalisations of the associated Legendre functions. The properties of this function $\boldsymbol{P_l^{mn}(\Phi)}$ as well as $\boldsymbol{T_l^{mn}(g)}$ are given in Bunge [8].

In Roe's notation, an ODF is expressed as follows:

$$f(\Psi\theta\Phi) = \sum_{\mathbf{l}=0}^{\infty} \sum_{\mathbf{m}=-\mathbf{l}}^{+\mathbf{l}} \sum_{\mathbf{n}=-\mathbf{l}}^{+\mathbf{l}} W_l^{mn} Z_{\mathbf{l}}^{\boldsymbol{mn}}(\cos\theta) \mathrm{e}^{-\mathrm{im}\Psi} \mathrm{e}^{-\mathrm{in}\Phi} \tag{2.8}$$

where W_l^{mn} are the series coefficients and $Z_l^{mn}\cos(\theta)$ is a generalization of the associated Legendre functions, the so-called augmented Jacobi polynomials.

Although the two methods are equivalent, henceforward, we shall be using only the Bunge's method (Eq. 2.7), which is more widely accepted.

A knowledge about the texture of a material can be obtained by knowing the value of the orientation distribution function $f(\varphi_1 \Phi \varphi_2)$ at different points within

the orientation space. The spherical harmonic functions $P_l^{mn}(\Phi)\, e^{-im\varphi_2}.\, e^{-in\varphi_1}$ in Eq. (2.7) are standard mathematical functions which can be calculated for all orientations, and these are usually stored in libraries [10, 11]. Therefore, an ODF can be completely described by knowing the values of the series expansion coefficients, C_l^{mn}. The objective here is to find the value of the coefficients namely C_l^{mn} (Bunge's notation) or W_l^{mn} (Roe's notation) that fit the pole figure data.

The values of C_l^{mn} can be calculated from the same data which are used to determine a pole figure. This can be illustrated as follows:

By virtue of the fact that a crystal is three dimensional, in order to describe the orientation of the crystallite uniquely, we need three angular parameters.

The relative frequency (or volume fraction) of crystallites within the sample, $\frac{\Delta v}{v}$, having the orientation defined by the set of angles $\alpha\ \beta\ \gamma$ within the limits of $\mathrm{d}\alpha\ \mathrm{d}\beta\ \mathrm{d}\gamma$, can then be written as

$$\frac{\Delta v}{v} = f(\alpha\ \beta\ \gamma)\ \mathrm{d}\alpha\ \mathrm{d}\beta\ \mathrm{d}\gamma \tag{2.9}$$

Here, γ is the angle about which a pole defined by an angle (α, β) in a two-dimensional pole figure can be rotated to represent the third dimension, keeping its angular location invariant. By definition, $f(\alpha\ \beta\ \gamma)$ is nothing but the orientation distribution function. This function can also be represented as $f(\varphi_1, \Phi, \varphi_2)$ where φ_1, Φ, φ_2 are the Euler angles.

A pole figure is the integral (or mean value) of the orientation distribution function (or ODF) taken over the angle γ. If P_{hkl} (α, β) is the pole density for the particular pole þ in the pole figure, we can write

$$P_{hkl}(\alpha, \beta) = \frac{1}{2\pi} \int_0^{2\pi} f(\alpha\beta\gamma)\mathrm{d}\gamma \tag{2.10}$$

$$\text{Or,} \qquad P_{hkl}(\alpha, \beta) = \frac{1}{2\pi} \int_0^{2\pi} f(g)\mathrm{d}\gamma \tag{2.11}$$

where $g = g(\varphi_1, \Phi, \varphi_2)$.

The pole figure is thus a two-dimensional "projection" of the three-dimensional ODF. The Eq. (2.10) essentially shows that we should be able to calculate an ODF from the pole figure data. This equation therefore represents the "fundamental equation for the computation of ODF." The method of deriving an ODF from pole figures is known as "pole figure inversion."

2.3.3 Pole Figure Inversion Using Series Expansion

In the series expansion method, it is assumed that both the measured pole figures and the ODF derived from those can be fitted by series expansions, using suitable

mathematical functions. In this scheme, the ODF $f(\varphi_1, \Phi, \varphi_2)$ can be expanded in a series of generalized spherical harmonic functions, $T_l^{mn}(\varphi_1\ \Phi\ \varphi_2)$ such as:

$$f(\varphi_1 \Phi \varphi_2) = \sum_{l=0}^{\infty} \sum_{m=-l}^{+l} \sum_{n=-l}^{+l} C_l^{mn} T_l^{mn}(\varphi_1 \Phi \varphi_2) \tag{2.12}$$

As mentioned earlier, since $T_l^{mn}(\varphi_1 \Phi \varphi_2)$ can be calculated for all orientations (φ_1, Φ, φ_2), the ODF $f(\varphi_1, \Phi, \varphi_2)$ can be completely described by knowing the values of the series expansion coefficients C_l^{mn}.

In a manner similar to the orientation distribution function, the pole figures can also be expanded in series expansion. Since an orientation in a pole figure is characterized by two angles α and β, a pole figure can be expanded in a series of spherical harmonic functions, $K_l^{mn}(\alpha,\ \beta)$ such as:

$$P_{hkl}(\alpha, \beta) = \sum_{l=0}^{l\text{max}} \sum_{n=-l}^{+l} F_l^n(hkl) K_l^n(\alpha, \beta) \tag{2.13}$$

where $F_l^n(hkl)$ are the series expansion coefficients and $K_l^{mn}(\alpha,\ \beta)$ are the spherical harmonic functions.

The coefficients $F_l^n(hkl)$ are related to the C_l^{mn} coefficients by the relationship:

$$F_l^n(hkl) = \frac{4\pi}{2l+1} \sum_{m=-l}^{l} C_l^{mn} K_l^{*m}(hkl) \tag{2.14}$$

where K_l^{*m} is the complex conjugate of K_l^m. The Eq. (2.14) forms a system of linear equations which can be solved to determine the values of the coefficient C_l^{mn}. Once the C_l^{mn} values are derived, the orientation distribution function $f(\varphi_1, \Phi, \varphi_2)$ can be calculated for any value of (φ_1, Φ, φ_2).

The series expansion given in Eq. (2.12) is a general one and does not take the symmetries of the specimen and the crystal structure of the material into account. In the presence of such symmetries, a modified function $T_l^{mn}(g)$ is to be used to fulfill the symmetry conditions.

Once this is done, it will reduce the number of coefficients needed to calculate the ODF. In Table 2.1, the total number of coefficients needed to evaluate the ODF have been given vis-à-vis the number of coefficients required when the symmetry conditions are considered.

2.3.4 Problems with the Series Expansion Method

An ODF computed by the series expansion method, as described above, may contain two serious errors, namely (1) truncation error and (2) ghost error. The truncation error arises mainly due to the fact that the series expansions represented by the Eqs. (2.2), (2.3), (2.9), and (2.10) have to be truncated to a limited number of terms to keep the computation time to practical limits. In all those equations, the

Table 2.1 Total number of coefficients C_l^{mn} (without symmetry) and $C_l^{\mu\nu}$ (cubic–orthorhombic symmetry) up to $l = \mathrm{L}$. After [8]

L	C_l^{mn}	$C_l^{\mu\nu}$
0	1	1
4	165	4
10	1771	24
16	6545	79
22	16215	186

summations are controlled by the index l, which, in other words, means that the maximum value of $l_{\max}$ used to calculate the value of the series expansions will determine the extent of this error. In practical terms, a value of $l_{\max} = 22$ is generally taken as a limit for cubic materials, whereas for very sharp textures, a value of $l_{\max} = 34$ is considered to yield sufficiently accurate results.

The second, more severe error is the so-called ghost error. Very often, in an ODF, orientation intensities may be missing in some locations where these should have been, or wrong orientation intensities can appear in some locations, where these should not have been. The former is known as negative ghost, whereas the latter is known as positive ghost. It appears that these ghosts are caused by the lack or absence of the odd-order series expansion coefficients, C_l^{mn}. A complete ODF, $f(g)$ in fact, is composed of two parts, which can be written as

$$f(g) = \bar{f}(g) + \bar{\bar{f}}(g) \tag{2.15}$$

where $\bar{f}(g)$ is defined by the even-order C-coefficients and $\bar{\bar{f}}(g)$ is derived from the odd-order C-coefficients. While the first term $\bar{f}(g)$ can be obtained from the diffraction pole figures, the second term $\bar{\bar{f}}(g)$ cannot be so obtained. Because of the fact that the odd-order C-coefficients assume a value zero for low l and have quite small values for large l, the impact of the $\bar{\bar{f}}(g)$ term will be limited in practice, and the error involved in calculating $f(g)$ without the $\bar{\bar{f}}(g)$ has been estimated to be about 20 %. In order to derive a complete ODF, by correcting for the ghosts, the term $\bar{\bar{f}}(g)$ has to be determined. In general, the procedures adopted to derive the odd-order C-coefficients assume that the ODF is non-negative for all orientations, i.e., $f(g)$ must be greater than zero, whatever be the orientation. The different methods for deriving ghost-corrected ODFs, so far suggested, are the "zero-range method" [13, 14], the "quadratic method" [15], the "positivity method" [16, 17], the "maximum entropy method" [18–21], and the method proposed by Lücke et al. [22, 23] in which the experimental ODF is deconvoluted into a set of several individual orientations, from which a model ODF is calculated by assigning a Gaussian scatter around each orientation. This last method produces a reasonably ghost-free complete ODF, based on both the even-order and odd-order C-coefficients.

2.3.5 Pole Figure Inversion Using Direct Methods

In addition to the series expansion methods, described above, some rather direct methods of ODF calculation have been proposed, which can derive the ODF $f(g)$ directly from the pole figure data.

In all these methods, the orientation distribution function $f(g)$ is considered only at discrete orientations g_j in the orientation space. Similarly, the pole figure $P_{hkl}(\alpha, \beta)$ is considered at a finite number of discrete points $(\alpha, \beta)_i$. In practice, both the pole figure and the orientation space are divided into regular grids with spacing of 2.5° or 5°. Under the considerations of crystal geometry, a relation between the individual points in the pole figure and the corresponding orientation cells in the orientation space can now be easily established. In fact, the integral Eq. (2.11) can now be replaced by a finite summation for each point $(\alpha, \beta)_i$ of the pole figure, as shown below:

$$P_{hkl}(\alpha, \beta)_i = \sum_{j=1}^{j} J_{ij} f(g_j) \tag{2.16}$$

The Eq. (2.16) describes a set of linear equations which can be solved, under appropriate conditions, to yield the orientation distribution function $f(g)$. From the initially estimated ODF, the fit between the ODF values at the discrete orientations and the values at the associated individual pole figure points is continuously improved by using an iterative procedure.

Some of the important direct methods to calculate an ODF are (1) the WIMV method, named after Williams [6] and Imhof [24] who developed it, and which was later improved by Mathies and Vinel [25, 26]; (2) the vector method, developed by Ruer and Baro [27] and by Vadon and Heizmann [28]; (3) the component method, developed by Helming and Eschner [29]; and (4) the arbitrary defined cells (ADC) method, developed by Pawlik [30], Pawlik et al. [31], and which is based on the WIMV method. The reader can go through the relevant literature to learn the details of all the above methods. Figure 2.14 shows the flow chart of ODF calculation, developed according to the WIMV method [32].

The methods to calculate ODFs from pole figure data have now been developed to quite an advanced stage, so much so that if good experimental data are available, it is possible to routinely yield reliable and reproducible ODFs. However, in general, the direct methods of ODF calculation require fewer pole figures, as compared to the series expansion methods, for obtaining ODFs of satisfactory quality, and this may be of particular interest while examining low-symmetry materials. On the credit side of the series expansion methods, their major output are the C-coefficients, which characterize the texture completely, and which can be more easily stored than the entire ODF data. In addition to the information pertaining to orientation distribution in a polycrystalline material, additional information on texture-related properties can be derived from the C-coefficients by using them in appropriate equations.

2.4 Representation of Texture in the Orientation Space

As mentioned already, the three-dimensional orientation space is defined by three Euler angles φ_1, Φ, and φ_2 (Bunge notation). Any orientation (of a crystal or grain in a polycrystalline material) can be specified within this space by a point,

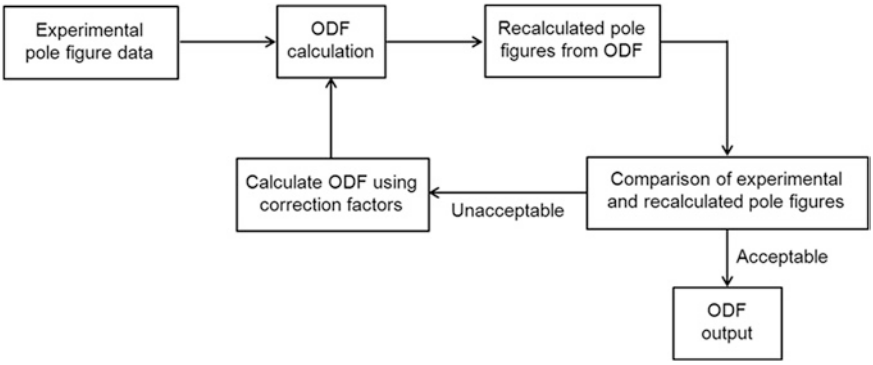

Fig. 2.14 Flowchart showing the procedure for calculating the orientation distribution function

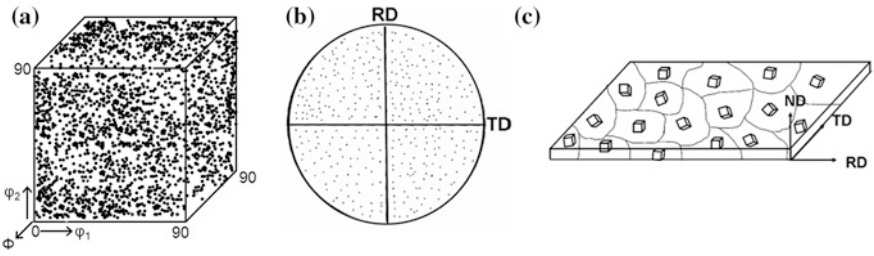

Fig. 2.15 Schematic representation of random distribution of orientations in **a** Euler space, **b** pole figure, and **c** crystallites in a rolled sheet

which will have a unique set of φ_1, Φ, and φ_2 values. The orientation distribution function $f(g)$ essentially describes a density distribution in the three-dimensional orientation space. It is for this reason why texture analysis involving orientation distribution function is known as "three-dimensional texture analysis."

A typical three-dimensional orientation space for a polycrystalline material with random orientation will display a uniform distribution of points in the Euler space (Fig. 2.15a). The corresponding pole figure and crystallite distribution in a sheet material is presented in Fig. 2.15b, c. On the other hand, for a strongly cube-textured sheet, the orientation distribution will be localized at the corners of the Euler space (Fig. 2.16a). The pole figure and the corresponding arrangement of crystallite in a sheet material are also presented in Fig. 2.16b, c. These are, however, extreme cases and are hardly realized in actual practice. In most practical situations, there is a distribution of intensities in the Euler space. The description of texture components is accomplished by locating the local maximum values of $f(g)$ in the orientation space.

The size of the orientation space, necessary to represent all possible orientations, is determined by the specimen and the crystal symmetries. For example, for a material crystallizing in the cubic system (cubic symmetry) and for a sheet

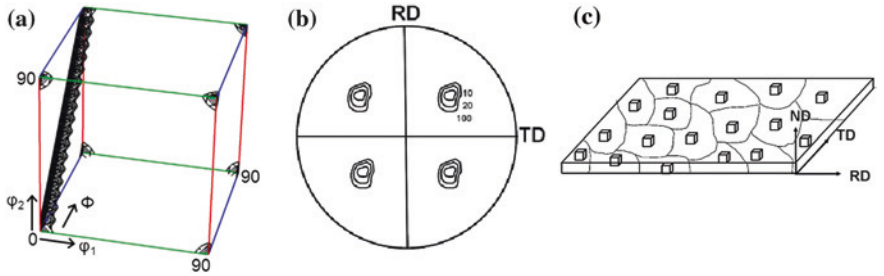

Fig. 2.16 Schematic representation of a strongly cube-textured material in **a** Euler space, **b** pole figure, and **c** crystallites in a rolled sheet

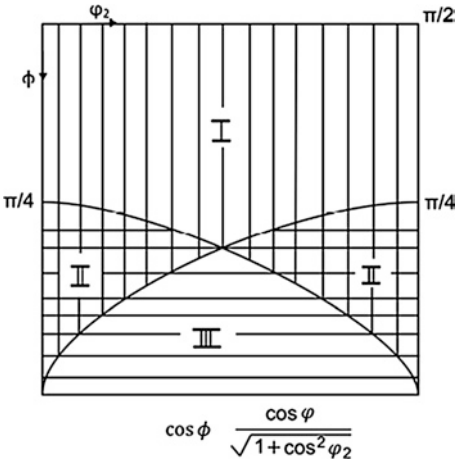

Fig. 2.17 ODF section displaying three equivalent regions owing to the threefold symmetry of cubic crystals. After [12]

sample (orthorhombic symmetry), a cubic orientation space defined by $\varphi_1 = 0°$–$90°$, $\varphi = 0°$–$90°$, $\varphi_2 = 0°$–$90°$ is what is needed to represent all possible orientations. One orientation can appear three times in this cubic orientation volume. In fact, this volume can again be subdivided into three symmetrically equivalent right prism-like parts, where one single orientation will appear only once in any one of the three parts. Here, the three basic volumes are indicated by different types of hatching (Fig. 2.17). Thus, for a cubic material, only one of the three prismatic regions, I, II, or III, will be needed to represent every possible orientation once and only once.

A schematic view of such a three-dimensional orientation space is shown in Fig. 2.18a, which also shows the locations of some important orientations or texture components. An actual three-dimensional orientation space depicting the variation of $f(g)$ is also shown in Fig. 2.18b. Since it is not very convenient to locate the positions of orientation maxima in such a three-dimensional diagram, it is customary to divide the three-dimensional orientation space into parallel two-dimensional sections and spread these sections on a piece of paper (Fig. 2.18c). The sections can be taken perpendicular to any of the φ_1, Φ, φ_2 axes.

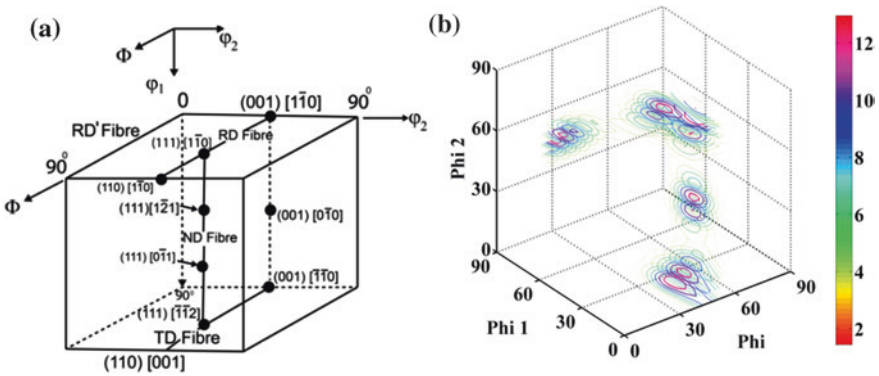

Fig. 2.18 **a** Three-dimensional Euler space representing important texture components. **b** Orientation distribution depicted in 3D for Ni–20Co alloy rolled to 98 %. **c** Corresponding 2D projection of φ_2 sections (*Courtesy* R Madhavan)

The important orientations for the deformation and recrystallization textures of FCC materials generally appear in the φ_2 sections, while the φ_1 sections show the major orientations connected with BCC materials. However, for researchers working on steels, the most important ODF section is the $\varphi_2 = 45°$ section. Figure 2.19a shows the φ_2-45° section of the ODF for a heavily cold-deformed sample of pure copper. Clearly, orientation density "peaks" can be seen in this diagram. By contrast, Fig. 2.19b shows the $\varphi_2 = 45°$ section of the ODF for a cold-rolled and annealed deep drawing quality steel. Obviously, here, the orientation density appears to lie along a line (called a "fiber") in the orientation space. An ODF plot can show both "peak"-type and "fiber"-type texture components. Some ideal texture components, normally encountered in steels, are presented in the $\varphi_2 = 45°$ section of the ODF in Fig. 2.19c.

The characteristic texture fibers that are normally encountered in FCC and BCC materials are depicted in Table 2.2. These fibers have also been indicated in Fig. 2.20a and b.

Specific differences in the rolling and recrystallization textures of different materials can be more clearly understood by plotting the pole densities along these fibers. It may be noted here that the course of the β fiber is not fixed in the Euler space, as in case of others fibers. In fact, the β fiber connects the pole density maxima in several ODF sections. For example, in FCC materials, the rolling texture at high deformation levels can be characterized by the β fiber which, in the Euler space, runs from Cu-orientation $\{112\}\ \langle 111\rangle$, through the S $\{123\}\ \langle 634\rangle$, ending up at the Brass orientation $\{110\}\ \langle 112\rangle$. Since the course of the β fiber is not fixed in the Euler space, it is more appropriate to call it as an "orientation tube," and the line depicting the axis of this tube is known by the term "skeleton line." Study of the details regarding the location of the β fiber in the Euler space in the rolling texture may yield valuable information about the underlying deformation mechanism. Figure 2.21a–c shows the α, β, τ fiber plots for a cold-rolled Ni_3Al + B alloy [35]. The amounts of cold deformation have been shown in the insets of these plots. It can be seen that the

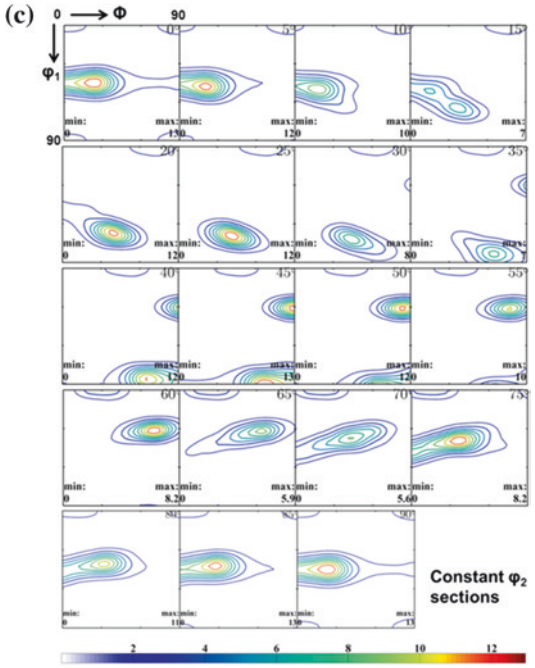

Fig. 2.18 continued

variation in $f(g)$ value along φ_1, Φ, or φ_2 can give an idea about the textural changes in the material as a function of the amount of deformation.

2.5 Volume Fraction of Texture Components

In quantitative texture analysis, it is often desirable to determine the volume fractions of different texture components. The volume fraction of a texture component is defined by

$$V_f(g) = \frac{\Delta V(g)}{V_{\text{total}}} \tag{2.17}$$

Here, $\Delta V(g)$ is the volume element corresponding to the orientation g and is related to the orientation distribution function in a given volume V, by the following expression,

$$\frac{\mathrm{d}V(g)}{V} = f(g)\mathrm{d}g \tag{2.18}$$

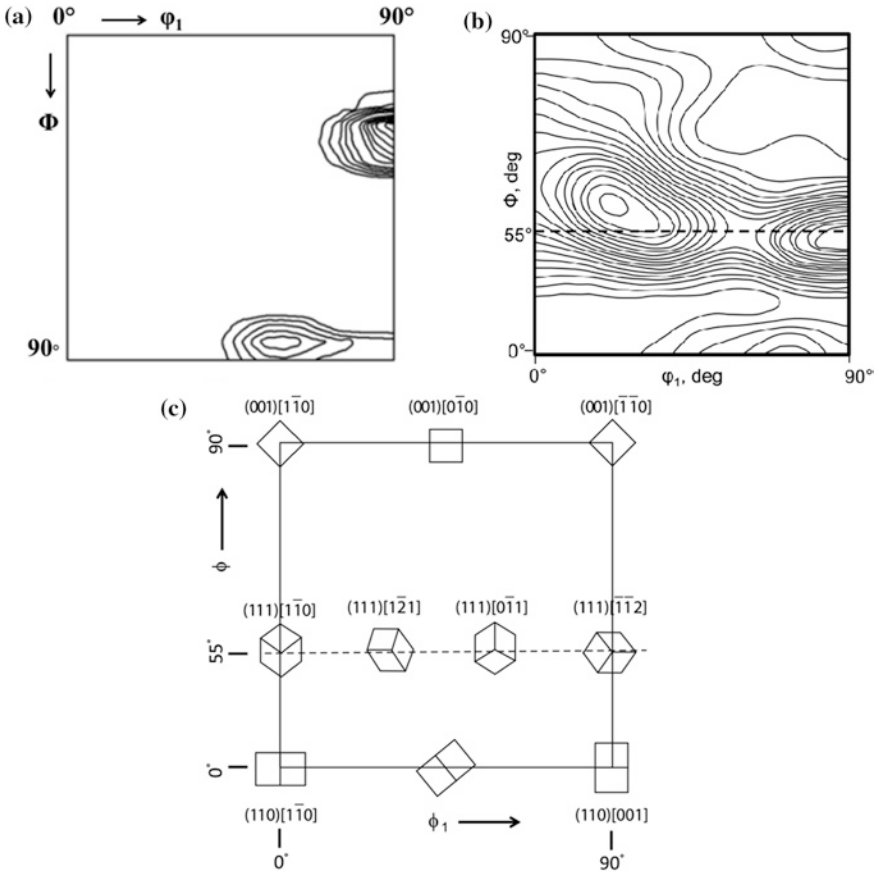

Fig. 2.19 **a** $\phi_2 = 45°$ section of the ODF for a cold-rolled copper (Courtesy: R Madhavan). **b** $\phi_2 = 45°$ section of the ODF for a cold-rolled and annealed deep drawing quality steel. **c** Ideal texture components located in $\phi_2 = 45°$ section. From [33]

Table 2.2 Texture fibers in FCC and BCC materials

Material	Nomenclature of fiber	Fiber axis
FCC	α	$\langle 110 \rangle \parallel$ ND
	γ	$\langle 111 \rangle \parallel$ ND
	τ	$\langle 110 \rangle \parallel$ TD
	β	Not a fiber in true sense
BCC	α	$\langle 110 \rangle \parallel$ RD
	γ	$\langle 111 \rangle \parallel$ ND
	η	$\langle 001 \rangle \parallel$ RD
	ξ	$\langle 110 \rangle \parallel$ ND
	ε	$\langle 110 \rangle \parallel$ TD

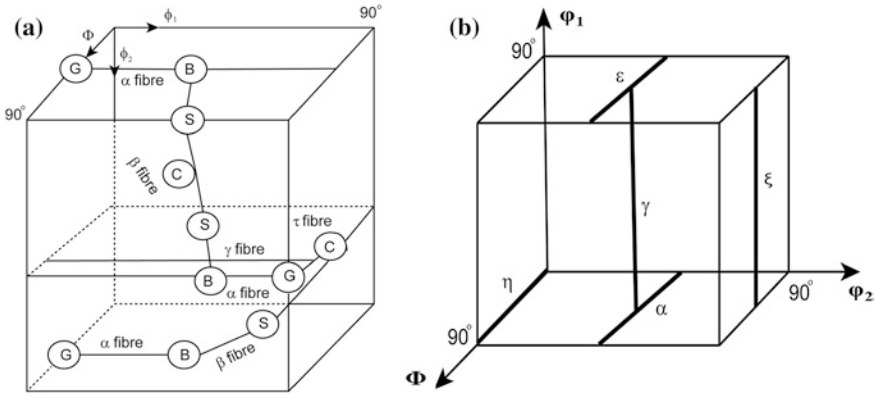

Fig. 2.20 Important texture fibers being embedded in the Euler space. **a** FCC [34]. **b** BCC [33]

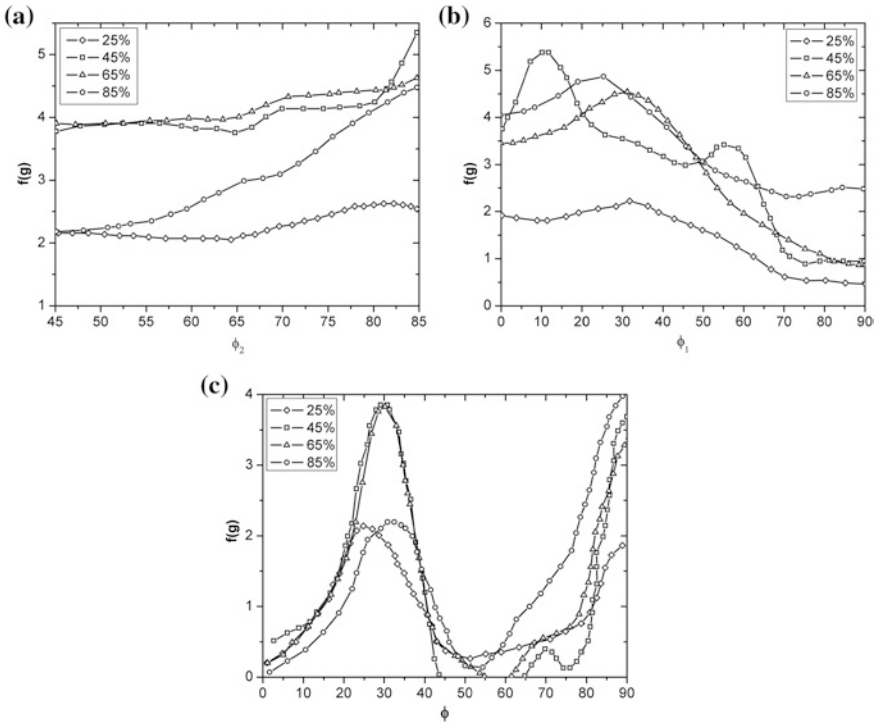

Fig. 2.21 Texture fiber plots for the cold-rolled Ni_3Al + B alloy. **a** α-fiber, **b** β-fiber, and **c** τ-fiber. After [35]

The volume fraction of the orientation g, defined by the three Euler angles (φ_1, Φ, φ_2), is given by

$$V_f(\varphi_1, \Phi, \varphi_2) = \int_{\varphi_1-\Delta\varphi_1}^{\varphi_1+\Delta\varphi_1} \int_{\Phi-\Delta\Phi}^{\Phi+\Delta\Phi} \int_{\varphi_2-\Delta\varphi_2}^{\varphi_2+\Delta\varphi_2} f(\varphi_1, \Phi, \varphi_2)\mathrm{d}g \tag{2.19}$$

$$\text{Or,} \quad V_f(\varphi_1, \Phi, \varphi_2) = \int\int\int f(\varphi_1, \Phi, \varphi_2) \sin\Phi \ \mathrm{d}\varphi_1 \mathrm{d}\Phi \ \mathrm{d}\varphi_2 \tag{2.20}$$

In practice, the volume fraction of a texture component located at (φ_1, Φ, φ_2) is calculated by integrating the value of $f(g)$ within a range of $\pm 5^\circ$ in the orientation space, though it can be customized based on the requirement.

References

1. Casato JC, Fricke WG (1987) Orientations of the Cubic Unit Cell and Tetrahedron. Textures Microstruct 7:85–93
2. Partridge P (1967) The crystallography and deformation modes of hexagonal close-packed metals. Int Mater Rev 12:169–194
3. Ray RK, Jonas JJ (1990) Transformation textures in steels. Int Mater Rev 35:1–36
4. Bunge HJ (1965) Zur darstellung allgemeiner texturen. Z Metallkd 56:872–874
5. Roe RJ (1965) Description of crystallite orientation in polycrystalline materials. III. General solution to pole figure inversion. J Appl Phys 36:2024–2031
6. Williams RO (1968) Analytical methods for representing complex textures by biaxial pole figures. J Appl Phys 39:4329–4335
7. Williams RO (1968) Representation of textures of rolled copper brass and aluminum by biaxial pole figures. Trans Metall Soc AIME 242:105
8. Bunge H (1987) Three-dimensional texture analysis. Int Mater Rev 32:265–291
9. Bunge HJ, Morris PR (1982) Texture analysis in materials science: mathematical methods. Butterworths, London
10. Pospiech J, Jura J (1974) Determination of orientation distribution function from incomplete pole figures. Z Metall 65:324–330
11. Wagner F, Bechlerferry E (1982) A generalized library program for texture calculations with even and odd coefficients. J Appl Crystallogr 15:122–125
12. Hansen J, Pospiech J, Lücke K (1978) Tables for texture analysis of cubic crystals. Springer, Berlin
13. Bunge HJ, Esling C (1979) Determination of the odd part of the texture function. J Phys Lett 40:627–628
14. Esling C, Bechlerferry E, Bunge HJ (1981) Numerical-calculation of the odd part of the texture function. J Phys Lett 42:141–144
15. Van HP (1983) The use of a quadratic form for the determination of nonnegative texture functions. Textures Microstruct 6:1–19
16. Dahms M, Bunge HJ (1988) A positivity method for the determination of complete orientation distribution functions. Textures Microstruct 10:21–35
17. Dahms M, Bunge HJ (1989) The iterative series-expansion method for quantitative texture analysis.1. Gen Outline J Appl Crystallogr 22:439–447

18. Wang F, Xu JZ, Liang ZD (1989) Determination of the ODF of hexagonal symmetry materials according to the maximum-entropy method. Textures Microstruct 10:217–226
19. Wang F, Xu JZ, Liang ZD (1992) Determination of the complete ODF of cubic system materials by the maximum-entropy method. Textures Microstruct 19:55–58
20. Schaeben H, Fundenberger JJ (1994) Particular solutions of the PDF-to-ODF inversion problem of texture analysis by large-scale mathematical programming. J Appl Crystallogr 27:177–189
21. Schaeben H, Siemes H (1996) Determination and interpretation of preferred orientation with texture goniometry: An application of indicators to maximum entropy pole- to orientation-density inversion. Math Geol 28:169–201
22. Lucke K, Pospiech J, Virnich KH, Jura J (1981) On the problem of the reproduction of the true orientation distribution from pole figures. Acta Metall 29:167–185
23. Lucke K, Pospiech J, Jura J, Hirsch J (1986) On the presentation of orientation distribution functions by model functions. Z Metall 77:312–321
24. Imhof J (1977) Determination of an approximation of orientation distribution function using one pole figure. Z Metall 68:38–43
25. Matthies S, Vinel GW (1982) On the reproduction of the orientation distribution function of texturized samples from reduced pole figures using the conception of a conditional ghost correction. Physica Status Solidi (B) 112:111–114
26. Matthies S, Vinel GW (1982) An example demonstrating a new reproduction method of the ODF of texturized samples from reduced pole figures. Physica Status Solidi (B) 112:115–120
27. Ruer D, Baro R (1977) Vectorial method of texture analysis of cubic lattice polycrystalline material. J Appl Crystallogr 10:458–464
28. Vadon A, Heizmann JJ (1991) A new program to calculate the texture vector for the vector method. Textures Microstruct 14:37–44
29. Helming K, Eschner T (1990) A new approach to texture analysis of multiphase materials using a texture component model. Crys Res Tech 25:203–208
30. Pawlik K (1986) Determination of the orientation distribution function from pole figures in arbitrarily defined cells. Physica Status Solidi (B) 134:477–483
31. Pawlik K, Pospiech J, Lucke K (1991) The ODF approximation from pole figures with the aid of the ADC method. Textures Microstruct 14:25–30
32. Kocks UF, Tome CN, Wenk HR (1998) Texture and anisotropy: preferred orientations in polycrystals and their effects on materials properties. Cambridge University, Cambridge
33. Ray RK, Jonas JJ, Hook RE (1994) Cold rolling and annealing textures in low carbon and extra low carbon steels. Int Mater Rev 39:129–172
34. Hirsch J, Lücke K (1988) Overview no. 76: mechanism of deformation and development of rolling textures in polycrystalline fcc metals—I. Description of rolling texture development in homogeneous CuZn alloys. Acta Metall 36:2863–2882
35. Ghosh Chowdhury S, Ray RK, Jena A (2000) Texture evolution during recrystallization in a boron-doped $Ni_{76}Al_{24}$ alloy. Mater Sci Eng, A 277:1–10
36. Chowdhury SG, Ray RK, Jena AK (1998) Rolling texture in the intermetallic compound $Ni_{76}Al_{24}$(B). Mater Sci Eng, A 246:289–301

http://www.springer.com/978-1-4471-6313-8

Crystallographic Texture of Materials

Suwas, S.; Ray, R.K.
2014, XIII, 260 p. 157 illus., 5 illus. in color., Hardcover
ISBN: 978-1-4471-6313-8